STUDY OF CROSS-SHORE PROFILES AT SOUTH COASTS OF THE CASPIAN SEA UNDER RAPID CHANGES IN WATER LEVEL

Hesamodin Enayati[1], Mohsen Soltanpour[1], Tomoya Shibayama[2], Ioan Nistor[3]

Coastal zone management needs the prediction of the changes in shoreline and coastal profiles, where the fluctuation of sea water level plays an essential role. Climate change and human activities have accelerated the fluctuation/falling of water levels in lakes and enclosed water basins. Using satellite images and cross-shore beach profiles at twelve monitoring stations along the southern coasts of the Caspian Sea, the effect of the rapid fall of water level on the nearshore morphology is studied in this research. Radiometric and atmospheric corrections are made on satellite images, and the NDWI index is used to increase the accuracy of the shoreline extraction. Comparing the accuracy of different methods, it is concluded that the Hands (1984) formula relatively better predicts the shoreline advancement rate due to lowering water level.

Keywords: Caspian Sea; Climate change; Water Level Fluctuation; Shoreline Change; Satellite Image; Cross-shore Profile

INTRODUCTION

One of the certain consequences of human-caused global warming is the increase of global sea levels, where the resulting inundation highly affects the low-lying areas. The erosion of sandy beaches is another global problem considering that at least 70% of sandy beaches around the world are recessional (Bird, 1985).

The effect of sea-level rise on nearshore morphology has been widely studied in past decades. Bruun (1954, 1962) provided a simple 2-dimensional (cross-shore) model between the sea level rise and shoreline retreat, based on the concept of the equilibrium beach profile. Rosati et al. (2013) modified the original Bruun Rule by an additive term, which includes an additive term for landward sediment transport to increase the shoreline retreat due to sea level rise. On the other hand, the literature shows limited research on the results of fluctuations in water levels on beach profiles. Studying the changes in cross-shore beach profiles, Hands (1984) examined shoreline movements under water level fluctuations in Great Lakes. Dean (1991) presented a non-dimensional equation for shoreline advancement due to lowering water levels. Ataei et al. (2018) analyzed several cross-shore profiles on the south coast of the Caspian Sea and modified the inverse Bruun Rule (1962) during sea level falls, adding a term for the onshore sediment transport.

The rate of the shoreline retreat can be easily extracted from satellite images. Grouping pixels by their spectral properties in different wavebands, the shorelines are detected from the collected satellite images (e.g., Lu and Weng 2007; Phinn et al. 2000). These methods have been widely used for automatic and semiautomatic shoreline detections and mapping. Some studies used a single-band image (e.g., Frazier and Page 2000), while others employed a band ratio (Guariglia et al. 2006) or a combination of reflective bands to improve the surface water detection (Du et al. 2012). Rokni et al. (2014) applied and compared different satellite-derived indexes to extract the surface water of Lake Urmia. The results demonstrated that the Normalized Difference Water Index (NDWI) is superior to other indexes with the highest accuracy. Do et al. (2019) estimated the sediment transport rate and shoreline changes using satellite images on the North Holland coast.

STUDY AREA AND FIELD MEASUREMENTS

Measured by a surface area of 372,000 square kilometers and a volume of 78,200 cubic kilometers, the Caspian Sea is the world's largest lake, which accounts for 40 to 44 percent of the total lacustrine waters of the world. The basin, located in a semi-arid area between the latitudes of 36°-47°N and longitudes of 47°-54°E, is surrounded by five countries, i.e. Russia, Kazakhstan, Turkmenistan, Iran, and Azerbaijan (Fig. 1). The deeper south basin, with the maximum depth of 1025 meters, contains 66 percent of the total water volume.

[1] Civil Engineering Department, K. N. Toosi University of Technology, No. 1346, Vali-Asr St., Tehran, Iran
[2] Civil Engineering Department, Waseda University, 1 Chome-104 Totsukamachi, Shinjuku City, Tokyo, 169-8050, Japan
[3] Civil Engineering Department, Ottawa University, 75 Laurier Ave. East, Ottawa, ON K1N 6N5, Canada

Figure 1. Caspian Sea

Historical data and installed gauges reveal the large fluctuation/falling of Caspian Sea water level in recent years, resulting in a unique case study of nearshore morphological evolution. These fluctuations can be highly related to the changes in the water balance components due to climate change, including precipitation, evaporation, and river discharges, in which about 80% of river inputs belong to Volga (Rodionov 1994).

Figure 2 represents the 80-year history of Caspian Sea water level. The sea level had gradually fallen before 1977 to its lowest level in the past 400 years, i.e., about 28.2 meters below the global sea level (Baltic datum), resulting in navigability problems in harbors and access channels. However, an unexpected rise in the water level started in 1977 and continued up to -25.7 m in 1995 (about 2.5 meters). The rapid rise in the water level resulted in vast flooding in coastal areas of neighboring countries. After 1995, the sea level started to decrease again to its present level of about -27.4 m. Various scenarios of recent climate change models have suggested the future water levels between -28 m and -26 m by 2050 (Hoseini and Soltanpour 2020).
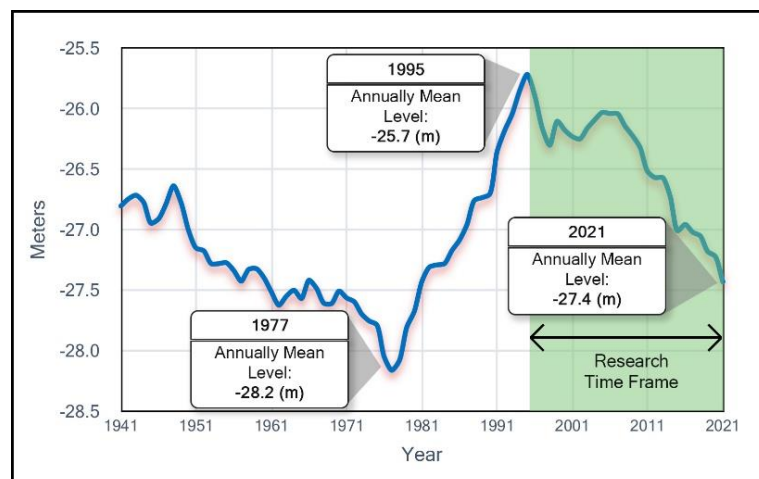

Figure 2. History of Caspian Sea water level

Figure 3 shows the existing monitoring stations along the south coast of the Caspian Sea. Satellite images and the periodic cross-shore profiles at these twelve stations are analyzed to study the impact of the recent falling water level (1995-2021) on the nearshore morphology.

Figure 3. Monitoring stations along the south coast of the Caspian Sea

METHODOLOGY

Equilibrium Cross-shore Profile

Literature shows a number of developed models to estimate shoreline changes and cross-shore beach profiles under water level fluctuations. Bruun (1962) suggested that the equilibrium profile will remain unchanged as the shoreline move landward and upward in response to rising sea levels (Eq. 1). In his conceptual model, a certain volume of sand moves from the upper part of the beach profile to accumulate on the lower part of the profile within the depth limit of the closure depth (Fig. 4). He assumed that the sand transport on the shoreface occurs solely through the interaction of particle water orbits and sand on the sea floor. In this study, the hypotheses of the Bruun rule are considered in a way suitable for estimating the shoreline changes due to lowering water level.

$$R = S\frac{W_*}{h_*+B} \qquad (1)$$

where R is the shoreline retreat, S is sea level rise, B is maximum run-up height, and h_* and W_* are the closure depth and active profile length after sea level change, respectively.
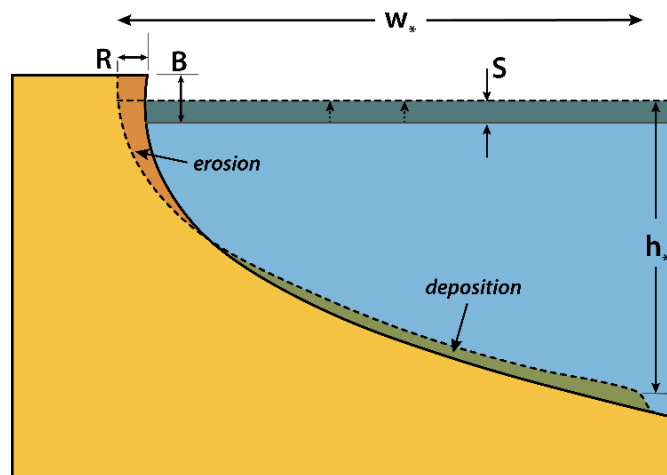

Figure 4. Characteristics of the Bruun Rule (1962)

Rosati et al. (2013) proposed a modified Bruun rule (Eq. 2), including an additive term to represent the landward sediment transport, which increased the shoreline retreat with respect to the equilibrium beach profile (Fig. 5). His modification increases the accuracy of prediction of the shoreline change under falling of water level.

$$R = S \, \frac{W_* + {V_D}/{S}}{h_* + B} \tag{2}$$

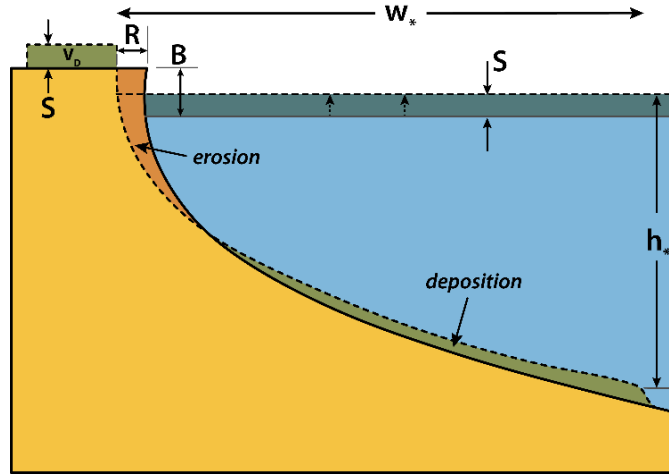where V_D is the volume per unit length of the landward deposition.

Figure 5. Variables in the modified Bruun rule (Rosati et al., 2013)

Following Rosati's hypotheses, Ataei et al. (2018) analyzed a large number of cross-shore profiles at the southern coasts of the Caspian Sea. He applied a coefficient to Rosati's formula to predict the shoreline change due to the falling of water level (Eq. 3).

$$\Delta y = A_S \, [S \, \frac{W_* + {V_D}/{S}}{h_* + B}] \qquad\qquad A_S = 2.963 \times 10^{-4} [\frac{H_B}{D_{50}}] \tag{3}$$

in which Δy is shoreline advancement and A_S coefficient depends on mean wave height in the breaker zone and the mean particle size of the bed (Fig. 6).
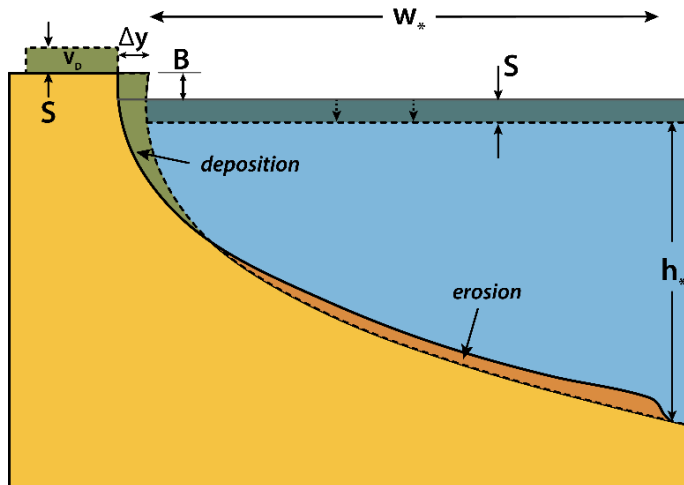

Figure 6. Variables in the modified Bruun rule (Ataei et al., 2018)

Dean (1991) presented a non-dimensional equation for the shoreline advancement under lowering water levels (Eq. 4).

$$\Delta y' = \frac{2}{5}\frac{(1 - S'B')^{\frac{5}{2}} - 1}{(B' - S'B' + 1)} \qquad \Delta y' = \frac{\Delta y}{W_*}, S' = \frac{S}{B}, B' = \frac{B}{h_*} \qquad (4)$$

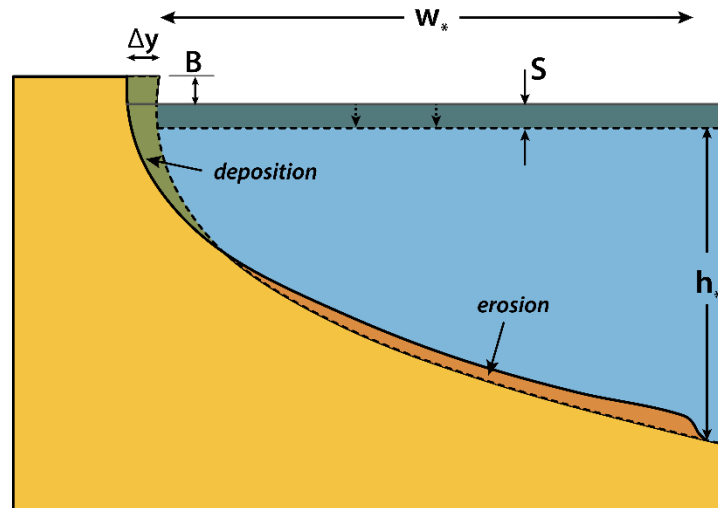where Δy is the shoreline advancement (Fig. 7).

Figure 7. Variables in the modified Bruun rule (Dean, 1991)

Hands (1984) studied the changes of cross-shore beach profiles and the shoreline movements in Great Lakes under water level fluctuations. The overfill ratio (R_A) was added to the Bruun rule to account for the impact of eroded sediments, moving out of the active zone (Eq. 5). He stated that under the water level rise, a percentage of the eroded sediments in the upper part of the beach profile moves out of the active zone, i.e., not accumulating in the lower part of the profile. Thus, more sediment is eroded from the upper part of the profile to create the equilibrium profile, which results in larger shoreline retreat. On the other hand, a part of the eroded sediment in the lower part of the profile is moves out of the active zone under the water level fall, i.e., not accumulating in the upper part of the beach profile. Therefore, less sediment is deposited in the upper part of beach profile, leading to less shoreline advancement (Fig. 8).

$$\Delta y = S \left[\frac{W_* \times R_A{}^{Sg(s)}}{h_* + B} \right] \qquad \begin{array}{l} Sg(S) = 1 \ \ \text{if} \ S > 0 \\ Sg(S) = \text{-}1 \ \ \text{if} \ S < 0 \end{array} \qquad (5)$$

Hands also added a term to account for the exit of longshore sediment from the active cell (Eq. 6).

$$\Delta y = S \frac{W_* \times R_A{}^{Sg(s)}}{h_* + B} - \frac{Qt}{(h_* + B)Y} \qquad (6)$$

where Δy is shoreline advancement, Y is the longshore length, and Q is the net exchange of sediment volume across the boundaries of the control area at time t.
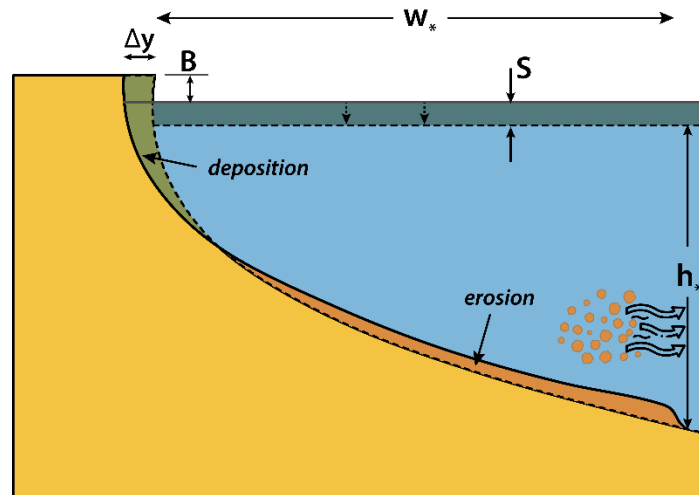
Figure 8. Variables in the modified Bruun rule (Hands, 1984)

Satellite Images

Thirty-two cloud-free images of Landsat 5 and 8 between May and June are employed to detect the satellite-derived shoreline of the south coast of the Caspian Sea (Fig. 9). Landsat 5 TM comprises seven spectral bands with a spatial resolution of 30 m for bands 1 to 5 and 7. The resolution of the thermal band (band 6) is 120 m which was resampled to 30-m pixels. Landsat 8 OLI and TIRS comprise eight bands with the spatial resolution of 30 m for bands 1 to 7 and 9, 15 m for Panchromatic band (band 8), and 100 m for two thermal bands (band 10 and band 11).
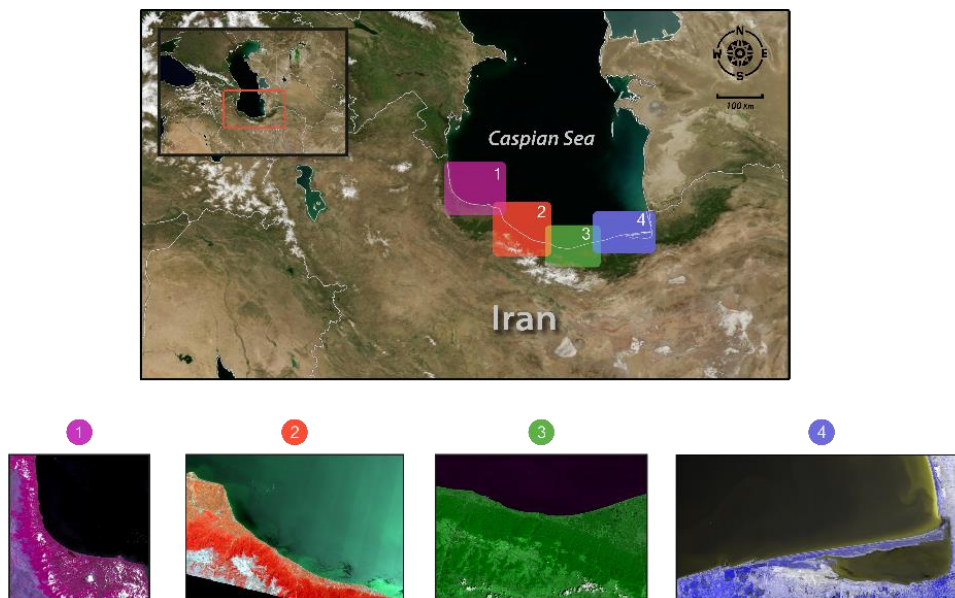

Figure 9. Cloud-free Landsat images of study area

The satellite-derived shoreline is defined by the position of the water-land boundary at the time of satellite imagery acquisition. An algorithm is applied to detect the shoreline position and its change rate. Figure 10 shows three steps of the applied algorithm to detect the shoreline position for the estimation of shoreline change., i.e.

1. Comprising radiometric calibration and atmospheric correction,
2. Extracting satellite-derived shorelines based on the NDWI value classification, using unsupervised classification techniques, and
3. Comparing the extracted shoreline positions in 1995 and 2021 at the shoreline segments by MATLAB.

The data records of different remote sensors in step 1 are not directly comparable because of the time differences in image acquisition, signal variations of exoatmospheric solar irradiance arose from spectral band distinctions, and atmospheric effects of aerosol scattering under various weather conditions on the image acquisition date (Kuleli et al. 2011). It is thus necessary to conduct radiometric calibration and atmospheric correction before extracting the shoreline position (Tyagi and Bhosle 2011). Step 2 presents the shoreline extraction, based on the classification of NDWI, to enhance the maximum distinction between land and sea (McFeeters 1996) (Eq. 7).

$$NDWI = \frac{\big(B(Green) - B(NIR)\big)}{\big(B(Green) + B(NIR)\big)} \tag{7}$$

where Green is the green band and NDWI is designed to:
1: maximize the reflectance of water using green wavelengths,
2: minimize the low reflectance of Near Infrared band (NIR) by water features, and
3: take advantage of the high reflectance of NIR by vegetation and soil features.

The algorithm results in enhanced positive values for water features, while the vegetation and soil have normally zero or negative values and are therefore suppressed (McFeeters 1996). Moreover, the NDWI technology can avoid the influence of the water content of vegetation leaves and the influence of floating leaved vegetation to extract the standing water content (Karsli, Guneroglu, and Dihkan 2011).

The unsupervised classification by the Iterative Self-Organizing Data Analysis Technique Algorithm (ISODATA) method is applied to identify the sea and land pixels. Thus, the pixels of the classified images shows only two values: land and sea. The changed values of pixels in step 3 are identified by comparing the classified images of 1995 with 2021 in shoreline segments. Finally, the rate of shoreline movement is obtained by examining the number of pixels with changed values in MATLAB.
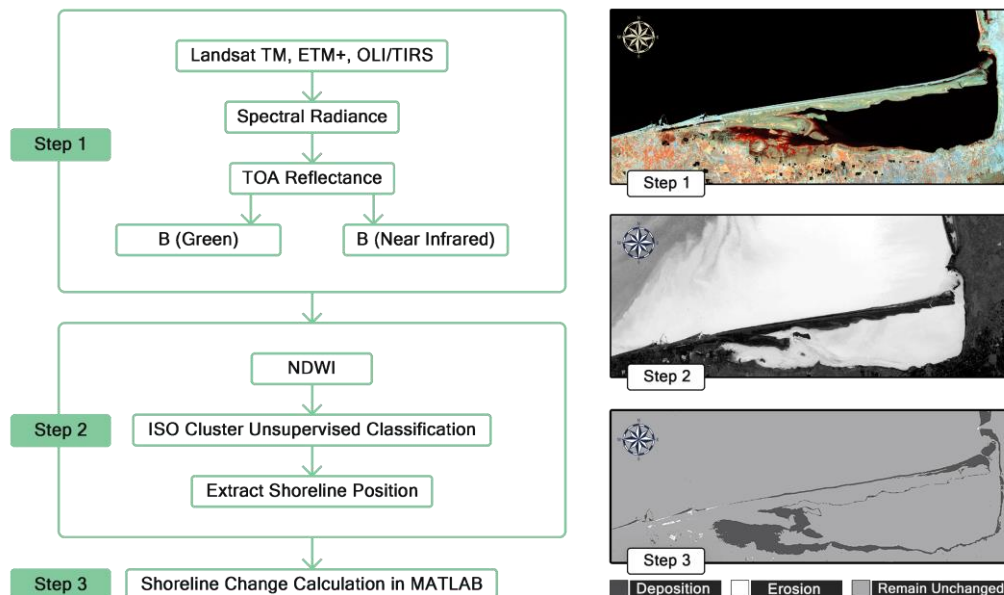

Figure 10. Processing to extract shoreline change from Landsat Images using Enhanced Thematic Mapper Plus (ETM+), Operational Land Imager (OLI) and Thermal Infrared Sensor (TIRS), Top-of-atmosphere reflectance (TOA reflectance)

RESULTS AND DISCUSSION

Figure 11 presents two samples of the evolution of beach profiles at Larim (top) and Miankaleh (bottom) stations during the falling water level from 2013 to 2021. The volumes of erosion/deposition are calculated by estimating the closure depth from the cross-shore profiles, assuming that an equilibrium profile is established. As an example of the outputs of the employed algorithm in MATLAB, Figure 12 (right) presents the rate of shoreline change at Miankaleh, in comparison to satellite images in GIS (left).
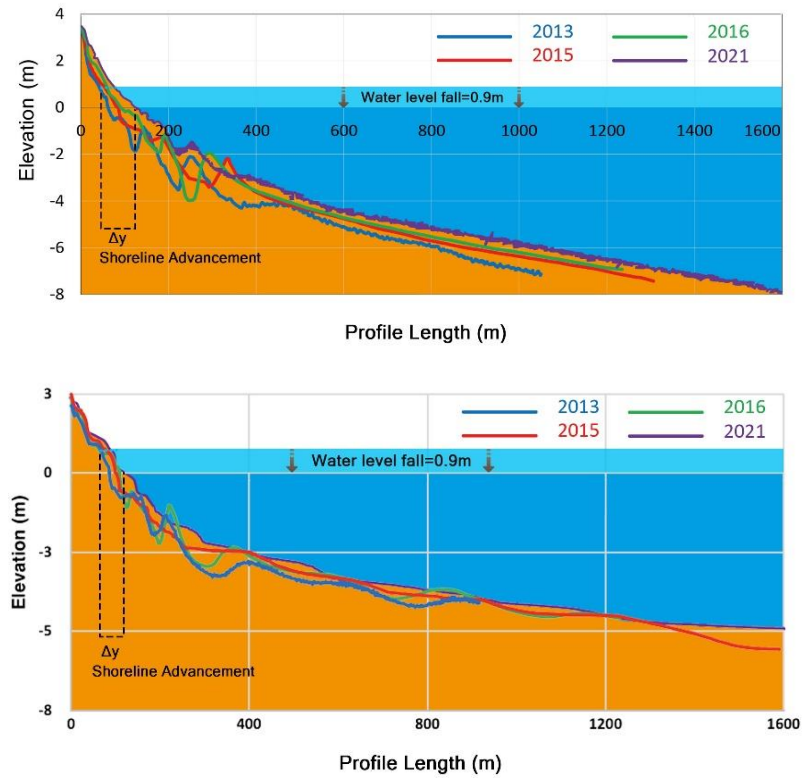
Figure 11. Cross-shore profiles at Larim (top) and Miankaleh (bottom) Stations
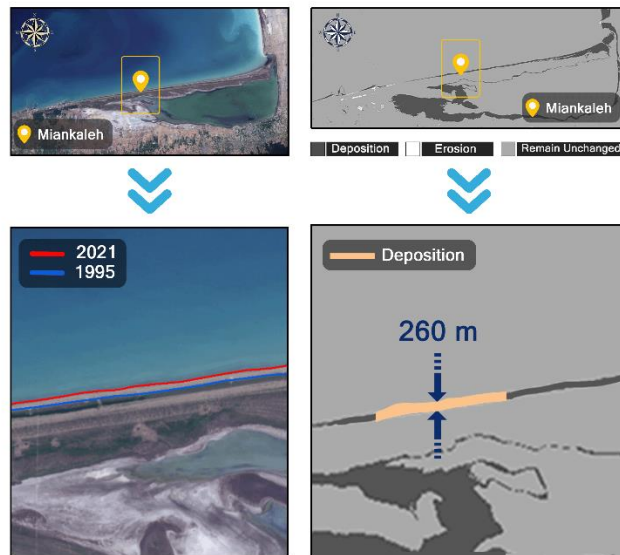

Figure 12. Shoreline change at Miankaleh (left: comparison of satellite images in GIS, right: developed algorithm in MATLAB)

Figure 13 presents the outputs of the shoreline change at measuring stations by different formulas, in comparison to the observed changes from the satellite images. Comparison of various methods can also be performed utilizing the statistical indices of Root Mean Square Error (RMSE) and Correlation Coefficient (Table 1).
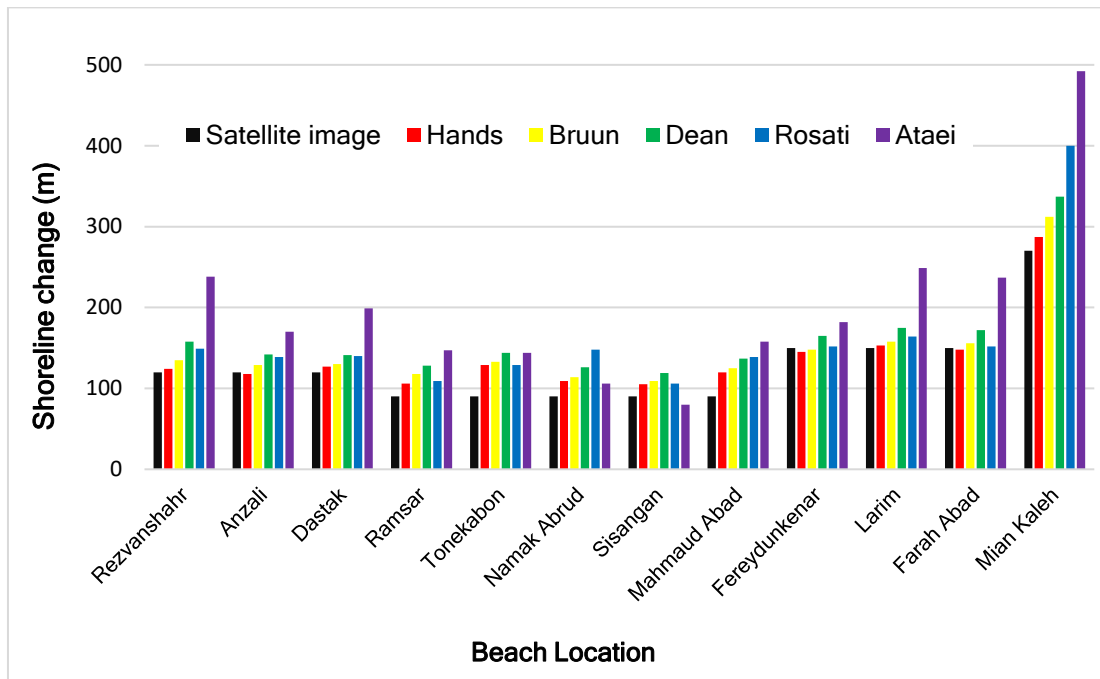
Figure 13. shoreline changes at measuring stations from 1995 to 2021

Method	RMSE (m)	Correlation Coefficient
Hands (1984)	19	1.27
Bruun (1962)	25	1.25
Dean (1991)	39	1.27
Rosati (2013)	49	1.22
Ataei (2018)	94	1.38

Table 1. Comparison of RSME and the correlation coefficient for applied formulas and observations

CONCLUSION

Measured profiles and satellite images at monitoring stations indicate the shoreline advancements due to lowering water level. All applied methods, i.e., Brunn (1962), Hands (1984), Dean (1991), Rosati et al. (2013), and Ataei et al. (2018), overestimate the shoreline advancement at monitoring stations, although the performance of Hands (1984) formula is relatively better. The existing differences in prediction might be related to the effect of longshore sediment transport, resulting in the change of sediment budget within the active sediment zone. A localized correction coefficient, related to the sediment diameter and wave climate, can be introduced to improve the prediction of future shoreline position at each station.

ACKNOWLEDGEMENT

REFERENCES

Ataei H, S., Adjami, M. and Neshaei, S.A. 2018. The effects of sea level fall on the Caspian Sea shoreline changes, *International Journal of Coastal and Offshore Engineering*, 3(3), pp.1-12.

Bird, E.C. 1985, *Coastline changes*. A global review.

Bruun, P. 1954. Coast erosion and the development of beach profiles (Vol. 44). US Beach Erosion Board.

Bruun, P. 1962. Sea-level rise as a cause of shore erosion, *Journal of the Waterways and Harbors division*, 88(1), pp.117-130.

Dean, R.G. 1991. Equilibrium beach profiles: characteristics and applications, *Journal of coastal research*, pp.53-84.

Do, A.T., Vries, S.D. and Stive, M.J. 2019. The estimation and evaluation of shoreline locations, shoreline-change rates, and coastal volume changes derived from Landsat images, *Journal of*

Coastal Research, *35*(1), pp.56-71.

Du, Z., Bin, L., Ling, F., Li, W., Tian, W., Wang, H., Gui, Y., Sun, B. and Zhang, X. 2012. Estimating surface water area changes using time-series Landsat data in the Qingjiang River Basin, China, *Journal of Applied Remote Sensing*, *6*(1), p.063609.

Frazier, P.S. and Page, K.J. 2000. Water body detection and delineation with Landsat TM data, *Photogrammetric engineering and remote sensing*, *66*(12), pp.1461-1468.

Giralt, S., Julia, R., Leroy, S. and Gasse, F. 2003. Cyclic water level oscillations of the KaraBogazGol–Caspian Sea system, *Earth and Planetary science letters*, *212*(1-2), pp.225-239.

Guariglia, A., Buonamassa, A., Losurdo, A., Saladino, R., Trivigno, M.L., Zaccagnino, A. and Colangelo, A. 2006. A multisource approach for coastline mapping and identification of shoreline changes, *Annals of geophysics*, *49*(1).

Hands. 1984. The great lakes as a test model profile response to sea level change, Coastal Engineering Research center, Department of the army, Waterways Experiment Station, Corps of Engineers PO Box 631.

Hoseini, S.M. and Soltanpour, M. 2020. LONG-TERM PREDICTION OF CASPIAN SEA LEVEL UNDER CMIP6 SCENARIOS USING ARTIFICIAL NEURAL NETWORKS, *Coastal Engineering Proceedings*, (36v), pp.5-5.

Karsli, F., Guneroglu, A. and Dihkan, M. 2011. Spatio-temporal shoreline changes along the southern Black Sea coastal zone. *Journal of Applied Remote Sensing*, 5(1), p.053545.

Kuleli, T., Guneroglu, A., Karsli, F. and Dihkan, M. 2011. Automatic detection of shoreline changes on coastal Ramsar wetlands of Turkey, *Ocean Engineering*, 38(10), pp.1141-1149.

Lu, D. and Weng, Q. 2007. A survey of image classification methods and techniques for improving classification performance, *International journal of Remote sensing*, 28(5), pp.823-870.

McFeeters, S.K. 1996. The use of the Normalized Difference Water Index (NDWI) in the delineation of open water features, *International journal of remote sensing*, 17(7), pp.1425-1432.

Phinn, S.R., Menges, C., Hill, G.J. and Stanford, M. 2000. Optimizing remotely sensed solutions for monitoring, modeling, and managing coastal environments, *Remote Sensing of Environment*, 73(2), pp.117-132.

Rodionov, S. 1994. Global and regional climate interaction: The Caspian Sea experience (Vol. 11), *Springer Science & Business Media.*

Rokni, K., Ahmad, A., Selamat, A. and Hazini, S. 2014. Water feature extraction and change detection using multitemporal Landsat imagery, *Remote sensing*, 6(5), pp.4173-4189.

Rosati, J.D., Dean, R.G. and Walton, T.L. 2013. The modified Bruun Rule extended for landward transport, *Marine Geology*, 340, pp.71-81.

Tyagi, P. and Bhosle, U. 2011. Atmospheric correction of remotely sensed images in spatial and transform domain, *International Journal of Image Processing*, 5(5), pp.564-579.